GEOPHYSICS, VOL. 77, NO. 1 (JANUARY-FEBRUARY 2012); P. P1–P10, 13 FIGS.
10.1190/GEO2011-0001.1

Flow noise reduction from superhydrophobic surfaces

Thomas Elboth[1], Bjørn Anders Pettersson Reif[2], Øyvind Andreassen[2], and Michael B. Martell[3]

ABSTRACT

This work investigates how a highly (super)hydrophobic surface can be used to reduce turbulence-generated drag and noise on a towed streamer cable. The work is done by analyzing full-scale drag and flow noise measurements taken on a commercial seismic streamer in combination with direct numerical simulations of turbulence-generated flow noise. The main findings are that viscous drag and flow noise can be significantly reduced on a seismic streamer that is coated to make the surface highly hydrophobic. In an ocean towing test, a 4% reduction of drag on a streamer section was measured. In a separate test on a commercial seismic vessel, a reduction in the flow noise level of nearly 50% (6 dB) for frequencies below 10 Hz was found. Based upon an analysis of numerical simulation data, it is suggested that the reduction in drag and noise can be attributed to a reduced level of shear stress and change in the kinematic structure of the turbulence, both of which occur in the immediate vicinity of the highly hydrophobic surface.

INTRODUCTION

This paper presents full-scale measurements of turbulence-generated hydro-acoustics along a (super)hydrophobic surface (SHS), as well as analysis of direct numerical simulations (DNS) of the same phenomena. The work in this study mainly relates to towed hydrophone arrays (seismic streamers) used for subsurface hydrocarbon exploration, but the results also apply to other hydro-acoustic sensors. This paper demonstrates, for the first time, that it is possible to achieve significant flow noise reduction by using such surfaces.

The objective of this study is to investigate the effect of SHS surface coating on the underlying mechanisms of turbulence-generated flow noise and to quantify the effects using full-scale experiments in the ocean. The paper is organized into three main parts. First, a brief review of noise in seismic data is provided, followed by a short introduction into the topic of SHS. Second, our computational methodology and our real-life measurements used to quantify and understand the effects of SHS on flow noise generation are described. Finally, the results are discussed and concluding remarks are given.

Marine seismic exploration is normally conducted by towing flexible streamer cables in the ocean. These cables are equipped with a large number of pressure sensors (hydrophones) on which recordings are made from subsurface reflections of acoustic energy originating from within a pressure source (air guns towed behind the seismic vessel). A large number of such recordings are used to construct an image of the subsurface. Figure 1 shows a schematic drawing of a seismic operation where streamer cables with a typical diameter of 5.5 cm and length of up to 12 km are used. The relative motion between a streamer cable and the ocean creates a turbulent boundary layer (TBL) that surrounds the cable. Figure 2 depicts such a boundary layer in which a colored dye is released near the streamer surface for visualization purposes. The noise generated by the fluctuating velocity and pressure fields within this TBL can significantly degrade the quality of data collected (Elboth et al., 2010).

Sources of underwater noise with frequencies ranging from zero to hundreds of kilohertz are discussed in the work by Wenz (1962), Kerman (1984), and recently, McDonald et al. (2008). The reference data used in these studies were mostly acquired from stationary nodes roughly 150 m below the ocean surface. Unfortunately, such stationary nodes do not record TBL flow noise.

Seismic subsurface reflection data is normally limited to the 2–250 Hz range. For the seismic industry, this is where the signal-to-noise ratio (S/N) primarily needs to be improved. Examples of noise sources within this frequency range include wave motion from surface waves, wakes from the towing vessel, and external currents that cause pressure fluctuations and rattling on streamer cables. Other noise sources include motion caused by swells that

Manuscript received by the Editor 5 January 2011; revised manuscript received 12 August 2011; published online 23 February 2012.
[1]Fugro Geoteam AS, Oslo, Norway. E-mail: t.elboth@fugro.no.
[2]Norwegian Defense Research Establishment (FFI), Kjeller, Norway. E-mail: reif@ffi.no; oya@ffi.no.
[3]University of Massachusetts, Department of Mechanical and Industrial Engineering, Amherst, Massachusetts, USA. E-mail: mmartell@ecs.umass.edu.

abruptly alter the towing vessel's speed and the presence of seismic equipment such as communication gear and depth controllers along the streamer cable.

Various types of ambient noises that propagate over long distances are also common. Examples are seismic interference, noise from oceanic traffic, and noise from marine creatures. Early work to determine noise characteristics and identify sources of noise on seismic streamers was done by Schoenberger and Mifsud (1974) and Fulton (1985). Furthermore, in the 1990s a number of researchers (Peacock et al., 1983; Bjelland, 1993; Dowling, 1998) made significant contributions to the understanding of noise generation mechanisms on fluid-filled seismic streamers. Since then, the seismic industry has focused on systematically improving streamer system technology to reduce the effects of many of the identified sources of noise. With few exceptions like Nishi (1970) and Cipolla and Keith (2008), that present pressure measurements from towed arrays, and Knight (1996) who presents calculations for TBL sound propagation inside a streamer array, work toward these improvements has not focused on noise originating from the TBL. However, it has recently been shown by Elboth et al. (2010) and Kjellgren and Davidson (2009) that on modern seismic streamer cables, TBL generated noise is often significant. For frequencies below 20 Hz it is often the dominating source of noise. Consequently, to reduce noise levels further, the TBL flow noise must be addressed.

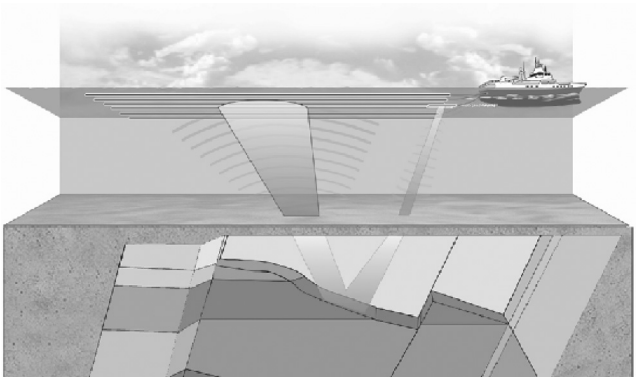

Figure 1. Illustration of a vessel that tows an air gun (energy source) and an array of hydrophones (seismic streamers). The air gun releases an energy pulse that propagates down into the subsurface where it is reflected at the interfaces between the different layers. The reflected energy is recorded by a large number of hydrophones mounted inside the streamer cables and used to reconstruct an image of the subsurface geology.

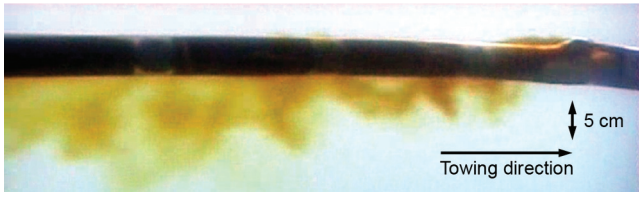

Figure 2. Image of parts of a seismic streamer with diameter $d \approx 5.5$ cm and towing velocity 4 knots. The TBL surrounding the streamer is revealed through the release of a dye close to the streamer surface. Details about this experiment can be found in Elboth et al. (2010).

A large number of approaches to develop surfaces that reduce drag have been considered in the literature. The use of bubbles (Sanders et al., 2006; Elbing et al., 2008), riblets (Choi, 1987; Bechert et al., 1997), polymers (Frohnapfel et al., 2007) and compliant walls (Hahn et al., 2002) are just a few examples. The relationship between drag reduction and radiated noise has also received some attention. The works by Barker (1973), Brungart et al. (2000), Winkel et al. (2008), and Elbing et al. (2010) have shown that wall pressure and the far-field noise level can be reduced in TBL that are modified by polymers or air-injection.

A recent promising approach to reduce drag involves the use of SHS coatings, initially inspired by the water repellent properties of the Lotus leaf (Barthlott and Ehler, 1977). On a microscopic scale, SHS are rough, with micrometer-sized surface features. In combination with chemical hydrophobicity, the material prevents water from moving into space between the peaks of the rough surface (Martell et al., 2010). The result is a surface with a mixture of no-slip and nearly shear-free regions at the microscale. Such surfaces have been shown to have water contact angles approaching 180°, and are referred to as superhydrophobic. On a macroscopic scale, a SHS will have, on average, a slip (nonzero) velocity, and have recently been shown to reduce surface frictional drag for laminar and turbulent flows (Henoch et al., 2006; Woolford et al., 2009). Of special interest to the work presented in this article is laboratory controlled experiments with turbulent flows by Daniello et al. (2009) which indicated up to 50% drag reduction on a carefully manufactured regular patterned SHS at turbulent, but relatively low Reynolds numbers. Also relevant is the work reported by Gogte et al. (2005) on drag reduction over a SHS with surface with random (made by sand paper) surface features. At $Re = 11000$, They reported a drag reduction of 7%, and observed that the same textured surface without the SHS coating showed several percent *increase* in drag compared to the untextured surface. At $Re = 11000$ a flow would be expected to be fully turbulent. However, it is still low compared to $\mathcal{O}(10^6$–$10^9)$ Reynolds number experienced by towed seismic streamer.

SIMULATIONS AND MEASUREMENTS

In this paper, two different approaches have been used to quantify the effects of SHS surfaces on flow noise generation. The first approach is based on an acoustic simulation and analysis of a DNS data of turbulent channel flow. The second approach takes the form of measurements using seismic streamer cables partly coated with a highly hydrophobic material. The computer simulation describes an ideal case that can help us to gain a physical understanding of the effects that govern the world of (super)hydrophobic drag and noise reduction.

Numerical simulations

The numerical analysis done in this work are based upon a $Re_\tau = u_* l/\nu = 395$ DNS of fully developed plane turbulent channel flow (Martell et al., 2009), which is described below. Here, $u_* \approx 0.04 U_0$ is the friction velocity, l is half the distance between the upper and lower walls that for the channel (channel height), U_0 is the centerline average velocity, and ν denotes kinematic viscosity. In numerical simulations of wall-bounded flows, it is normal to use Re_τ rather than $Re_L = UL/\nu$ as a measure for the Reynolds number.

Dette er en postprint-versjon / This is a postprint version.
DOI til publisert versjon / DOI to published version: 10.1190/GEO2011-0001.1

A $Re_\tau = 395$ corresponds to $Re_l \approx 10^5$ which gives fully developed turbulence.

Figure 3 shows the instantaneous velocity field from this flow simulation. Notice the stripes (ridges) on top of the channel. They illustrate the periodic slip and no-slip boundary conditions used to model the SHS-surface. Slip is implemented through a no-shear condition, *i.e.*, $(\partial u/\partial x_2)_{wall} = \partial w/\partial x_2)_{wall} = 0$, where u is the streamwise, w the spanwise (transverse) velocity, and x_2 the wall-normal direction. A no-penetration condition exists for the surface-normal velocity, $v = 0$. The imposition of these mixed wall boundary conditions constitutes a viable method to numerically model a SHS. A no-slip boundary condition is obtained by setting $u = v = w = 0$ at the wall. The bottom surface is a traditional no-slip boundary and the channel is periodic in the streamwise (x_1) and spanwise (x_3) directions.

In this direct numerical flow simulation, see Figure 3, the width in the spanwise direction of the alternating slip/no-slip areas on the top wall is 30 μm. This has been found to be a suitable size to represent the microscopic structure of a SHS. According to Martell et al. (2009), this slip/no-slip (SHS) boundary condition resulted in an slip velocity 45% of the mean velocity and an average shear stress reduction of nearly 15%. The results from this initial flow simulation are employed as input for an acoustical simulation, described in the next section.

Some caution about the applicability of the model to the real-world conditions is needed. At present, it does not account for the possibility the air trapped in the cavity regions of the SHS might be washed away by the high Reynolds number flow along a real-world seismic streamer, not to mention failure of the SHS due to large static pressures.

Acoustic simulations

This section describes the acoustic simulations employed to study the effect of SHS on flow noise. Flow noise on seismic streamers is generated by turbulent flow structures that propagate along the streamer surface with a velocity just below the towing speed (see Figure 2). The physical mechanisms responsible for flow noise generation were derived and explained by Lighthill (1952, 1954). Work more directly related to hydrophone array flow noise is presented by Haddle (1969). Flow noise generation can be expressed by the Lighthill inhomogeneous wave equation, which is derived without approximations from the Navier-Stokes equations. The equation states that the acoustic pressure fluctuations in a media are described by

$$\frac{1}{c_0^2}\frac{\partial^2 p}{\partial t^2} - \frac{\partial^2 p}{\partial x_i \partial x_i} = \frac{\partial^2 T_{ij}}{\partial x_i \partial x_j}, \tag{1}$$

where $T_{ij} = \rho u_i u_j - \sigma_{ij} + (p - c_0^2\rho)\delta_{ij}$, and c_0 denotes local speed of sound, which is considered to be constant in the model domain. The term $p(\mathbf{x}, \mathbf{t})$ is the instantaneous pressure and $\rho(\mathbf{x}, \mathbf{t})$ is the density of the fluid, which is nearly constant. Towed seismic streamers operate in a high Reynolds number flow environment. The viscous stresses, σ_{ij} and the feedback from the acoustic field to the flow field are therefore negligible. By assuming isentropic acoustic conditions, $p - c_0^2\rho = 0$, the momentum flux density tensor $\rho_0 u_i u_j$ for $i, j \in \{1, 2, 3\}$ is the dominating source in equation 1. A simplified Lighthill equation (Landau and Lifshitz, 1987) can be written as

$$\frac{1}{c_0^2}\frac{\partial^2 p}{\partial t^2} - \frac{\partial^2 p}{\partial x_i \partial x_i} = \rho_0 \frac{\partial^2 (u_i u_j)}{\partial x_i \partial x_j}. \tag{2}$$

Equation 2 can be solved numerically provided the second derivative of the tensor $u_i u_j$ is known. Note that $u_i u_j$ is comprised of products of velocity fluctuations in all three dimensions which vary in time. As an initial condition to balance equation 2, we used the fluctuating pressure field $p(\mathbf{x}, \mathbf{t})$. The spatially and temporally fluctuating velocity field from the channel-flow SHS simulation is used as the driving force, i.e., we apply a compressible correction from the solution on the direct numerical of *incompressible* flow.

Suitable acoustic boundary conditions must also be chosen to avoid unphysical reflections of waves from the outer boundaries of the computational domain. Reflected energy would quickly render any simulation data meaningless. In this study, we therefore use perfectly matched layers (PML) (Berenger, 1994) as boundary conditions. This method is a computationally efficient means of formulating an absorbing boundary. For computational reasons, it is convenient to rewrite the wave equation as a first-order pressure-velocity system

$$\frac{\partial^2 \dot{p}}{dt^2} = c^2 \left(\frac{\partial^2 \dot{p}_j}{\partial x_j \partial x_j} \right), \tag{3}$$

$$\frac{\partial p}{\partial t} = -c^2 \rho \left(\frac{\partial u_j}{\partial x_j} \right), \qquad \frac{\partial u_j}{\partial t} = \frac{-1}{\rho} \left(\frac{\partial p}{\partial x_j} \right). \tag{4}$$

Here, $\dot{p}(\mathbf{x}, \mathbf{t}) = \partial p/\partial t$ is the pressure field and $c = c(\mathbf{x})$ is the speed of sound. The term ρ denotes the density of the medium where the wave is propagating. Repeated indices imply summation. For simplicity, the source term (the right hand side of equation 2) is not shown here. However, this term needs to be included in the final PML formulation given in equation 5.

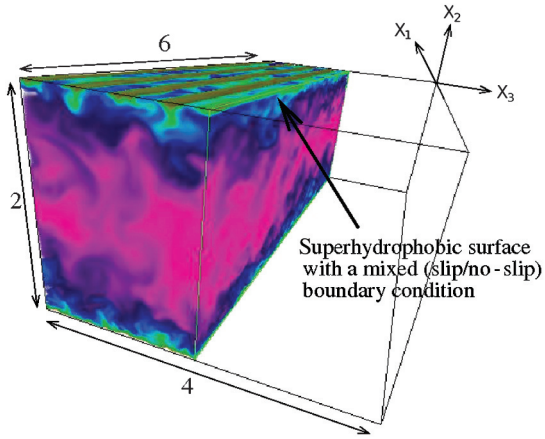

Figure 3. Visualization of the velocity magnitude in the DNS of channel flow over a SHS. A cut plane has been applied during visualization to better look at the interior of the data. The numbers two, four, and six in the figure indicate the relative size of the channel in the wall-normal (x_2), spanwise (x_3) and streamwise (x_1) directions, respectively. Physically, the channel size is $300 \times 600 \times 900$ μm. Flow velocities have been normalized to be in the 0–1 range. The 30 μm feature size of the mixed (slip/no-slip) boundary condition can be observed on the top of the channel.

Dette er en postprint-versjon / This is a postprint version.
DOI til publisert versjon / DOI to published version: 10.1190/GEO2011-0001.1

The PML method will now be briefly described. First, a change of variable is applied

$$\frac{\partial}{\partial x_3} \rightarrow \frac{1}{1 + i\sigma_{x_3}/\omega} \frac{\partial}{\partial x_3}.$$

Here, σ_{x_3} are the absorption coefficients in the wall-normal direction. The σ_{x_3}s are zero in the computational domain, and increase smoothly to one in the PML zone. The variable i represents the imaginary number and ω is the frequency. A periodic boundary condition is applied in the spanwise and streamwise directions.

In the frequency domain, equation 4 is multiplied by $(1 + i\sigma_{x_3}/\omega)$ and the variable change described above applied. Transformed back to the time domain, the PML formulation for 3D Cartesian coordinates becomes

$$\frac{-1}{c^2\rho}\frac{\partial p}{\partial t} = \frac{\partial u_j}{\partial x_j} - \sigma_{x_3} p, \qquad \rho\frac{\partial u_j}{\partial t} = \frac{-\partial p}{\partial x_j} - \sigma_{x_3} u_j. \tag{5}$$

Initial numerical tests showed that the absorbing PML-region needed to be at least 15 grid cells wide to avoid reflections. The acoustical simulations were conducted on an uniformly distributed grid consisting of $256 \times 512 \times 256$ cells in the streamwise, wall-normal and spanwise direction, respectively. High-order finite differences were used for the spatial derivatives, while a second-order accurate scheme was used in time.

Figure 4 displays a snapshot from the acoustic computation based in our DNS channel-flow database. The channel, with its acoustic sources, is shown as a semitransparent (gray) region within the larger computational domain.

The acoustic sources stem from the turbulent fluctuations, and are quadrupole in nature, i.e., their intensity reduces as $1/d^4$ with distance d from the source. This can be seen in Figure 4, where the flow intensity clearly weakens with distance from the channel surface. However, on a seismic streamer, where hydrophones are placed close to the outer streamer surface, quadrupole turbulent flow noise can still be strong.

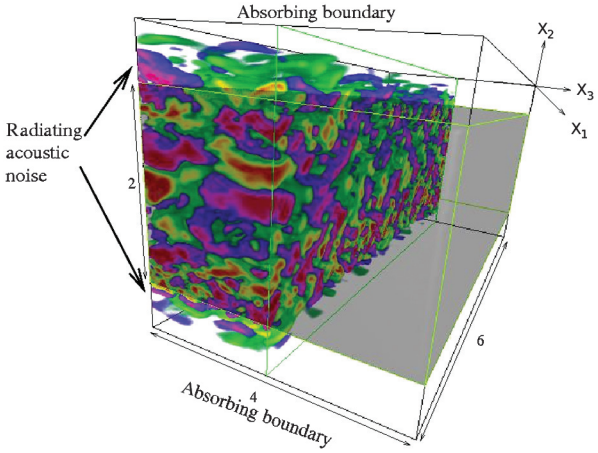

Figure 4. Visualizing flow noise: A snapshot from a simulation showing the acoustic pressure propagating out from turbulent flow features in the channel simulation. The positions of the absorbing acoustic boundary conditions are indicated in the figure. Red and blue (dark) indicate large amplitudes, while yellow and green (light) indicate weaker amplitudes. A cut-plane is applied to better reveal the characteristic structures of the noise. The numbers two, four, and six indicate the relative size of the simulation domain.

Analysis of numerical simulation data

The purpose of this section is to analyze the data from the DNS with the aim of understanding how the SHS affected the flow and the production of flow noise.

The top figure in Figure 5 shows the averaged first invariant of the T_{ij} tensor from equation 2, i.e., $T_{ii} = T_{11} + T_{22} + T_{33}$ (which is proportional to the turbulence kinetic energy). The bottom figure shows how the average rms pressure varies across the channel. It can be readily observed that both of these quantities are significantly reduced in the vicinity of the SHS. The dashed line in the bottom figure shows the ensemble average velocity across the channel. Notice that on the left (SHS) side, the (average) velocity does not approach zero at the boundary. The turbulent acoustic energy production only seems to be significant at a dimensionless wall distance $x_2^+ = yu_*/\nu < 50$. Here, x_2 denotes distance from the wall, $u_* \approx 0.04U_o$ is the friction velocity, and U_0 represents the free-stream velocity. This coincides with the area in which the Reynolds stresses and the turbulence production peak in boundary layer flows.

In physical coordinates, for a seismic streamer, $x_2^+ \approx 100$ corresponds to $x_2 \approx 1$ cm. This gives an indication of how close to a moving object flow noise production occurs.

The turbulence anisotropy is a measure of the directivity and magnitude of the turbulent fluctuations in a flow. Due to the partial slip boundary condition of the SHS, it is reasonable to assume the turbulence anisotropy will change close to this surface. The analysis below is done to investigate this change. The level of turbulence anisotropy can be quantified, following the analysis of Lumley and Newman (1977), by introducing

$$a_{ij} = \frac{\overline{u_i u_j}}{\overline{u_k u_k}} - \frac{1}{3}\delta_{ij}, \qquad i, j \in \{1, 2, 3\}. \tag{6}$$

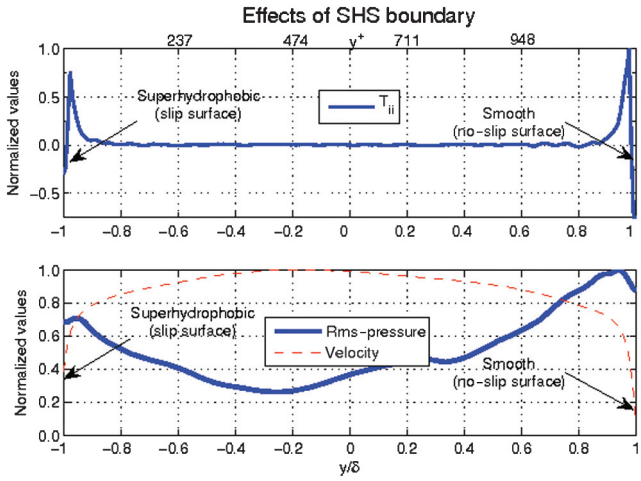

Figure 5. Top: Variation of the ensemble average first invariant of $T_{ii} = T_{11} + T_{22} + T_{33}$ tensor (solid) across the channel. The $x_2^+ = y^+$ coordinates are indicated in the top of the plot. Bottom: The ensemble average rms pressure (solid) and the ensemble average velocity (dashed) across the channel.

Dette er en postprint-versjon / This is a postprint version.
DOI til publisert versjon / DOI to published version: 10.1190/GEO2011-0001.1

Here, the overline denotes average quantities, while repeated indices imply summation. $\delta_{ij} = 1$ for $i = j$ and $\delta_{ij} = 0$ if $i \neq j$. The invariants of a_{ij} can be written as

$$I = a_{ii}, \tag{7}$$

$$II = a_{ij}a_{ji}, \tag{8}$$

$$III = a_{ij}a_{jk}a_{ki}. \tag{9}$$

In particular, the variation of II with III for axisymmetric turbulence can be written as

$$II = \frac{3}{2}\left(\frac{4}{3}|III|\right)^{2/3}, \tag{10}$$

whereas the corresponding relation for 2C turbulence is

$$II = \frac{2}{9} + 2III. \tag{11}$$

The second (II) and third (III) invariants define the anisotropy-invariant map according to Lumley (1978). Figure 6 shows the map where the closed curve bounds all physically realizable turbulence. In the same figure, we have also added two curves of a_{ij} corresponding to the variation of turbulence anisotropy from the walls and toward the center of the channel. This shows that the turbulence close to the SHS surface is significantly more anisotropic than the turbulence close to the no-slip surface, and that the kinematic structure of the turbulence is changed significantly by the SHS. It is particularly notable that the turbulence seems to approach a 1C limit in which the magnitude of one fluctuation is significantly larger than the other two. Physically, this implies that there is less turbulent mixing of momentum in the wall-normal direction close to the slip boundary. Consequently, less high-speed flow from the outer regions is brought into the low-speed near-wall region and the viscous drag is reduced.

Our observation fits well with results presented by Solbakken and Andersson (2004) and more recently by Frohnapfel et al. (2007) where they numerically studied the effects of long-chained polymers used for drag reduction in a channel. They found that drag reduction was associated with an increase in anisotropy near the wall, and that drag reduction effects of over 30% were possible when only a few points inside the viscous sublayer were forced toward high anisotropy.

Turbulence in a boundary layer is generated by the relative motion between the wall and the outer fluid. In this process, energy is transferred from the mean flow **U** to the turbulent field **u** by the action of the local velocity gradient (shear). The presence of a slip surface will reduce the turbulence intensity and wall friction (Woolford et al., 2009), while the mean velocity across the channel will increase. This can be quantified in a low Reynolds number flow from the DNS data.

In Figure 7, the relative magnitudes of the $\partial^2(\overline{u_i u_j})/\partial x_i \partial x_j$ components in equation 2 are compared from the wall and into the center of the channel. From this figure, it is clear that the magnitude of the acoustic source term is significantly reduced close to a SHS compared to the solid wall. The reduction is especially large for the components that have derivatives in the wall-normal direction, like e.g., $\partial^2(\overline{v}^2)/\partial x_2^2$. The wall-normal Reynolds-stress component in the vicinity of the SHS surface has been significantly reduced due to changes in the important pressure-redistribution process in the near-wall layer. The reduction of $\overline{v}^2$ results in less production of turbulent shear stress $\overline{uv}$ and thus also reduced turbulence kinetic energy.

Due to the slip condition on the SHS side of the channel, the turbulence statistics across the channel are not symmetric (Martell, 2009). A coupling between the wall and SHS regions can therefore be expected, which may affect the results somewhat. Nevertheless, the trends are very clear, which provide confidence in our understanding of how and why the flow noise level is reduced by the introduction of a SHS.

Visually, it is difficult to observe any difference in acoustic intensity between the top (SHS slip) and the bottom (no-slip) flow

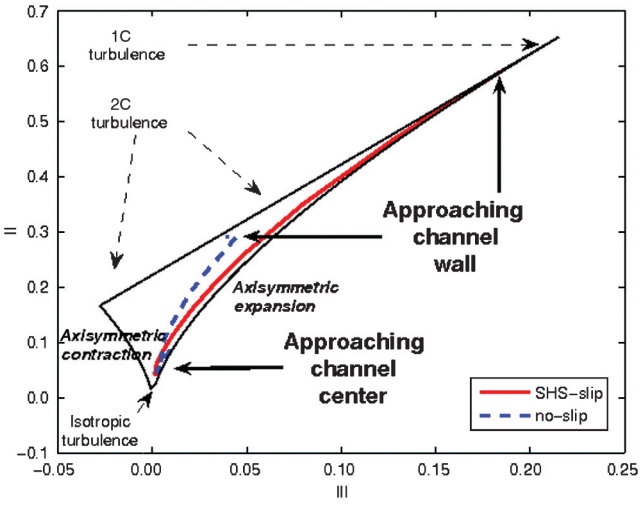

Figure 6. An anisotropy-invariant map showing the limiting states of turbulence and the variation of turbulence anisotropy from the channel center toward the solid and SHS boundaries of the channel.

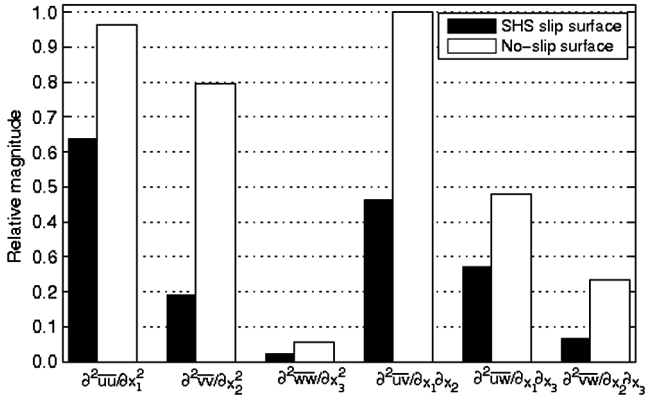

Figure 7. Data derived from the DNS of channel flow: Comparing the magnitude of the acoustic source term T_{ij} components from the wall and into the center of the channel. The effects of the SHS can clearly be observed. The six independent tensor components are shown along the x-axis.

Dette er en postprint-versjon / This is a postprint version.
DOI til publisert versjon / DOI to published version: 10.1190/GEO2011-0001.1

boundary in Figure 4. A better impression of the effects of the SHS in the simulation data is obtained by comparing 2D instantaneous pressure distributions outside the two boundaries (walls). This is shown in Figure 8. Note how the amplitudes (the variations in surface height) are much larger outside the normal no-slip surface (left), compared to outside the SHS-surface (right). To compare the simulation results with real seismic noise records, it becomes necessary to model the effects of the pressure fluctuations on a hydrophone sensing area. A hydrophone area was modeled by averaging the pressure over a 2 cm × 1 cm area in a time series, 0.5 cm outside the SHS slip and the normal no-slip boundary. The difference in temporal rms between these two simulated hydrophones was almost 60%, which illustrates the effects an ideal SHS can have on the flow noise level.

Measurements on a seismic streamer cable

The literature describes a large number of approaches to produce SHS. See, for example, the work by Ma and Hill (2006). A convenient and inexpensive way to make a surface (super)hydrophobic is to apply a suitable coating material. The coating material used in this experiment is one delivered by the company NC Norge AS. It consists of a silane blend mixed with isopropanol and ethanol. The fluid is sprayed onto a surface where it forms a pattern. According to the manufacturer, water contact angles up to 150° have been measured. In our experiments using seismic cables made from polyurethane (PU), the contact angle measured through a PC-controlled camera microscope was in the order of 110°–120°. Untreated PU has a contact angle of around 75°. The top image in Figure 9 shows scans of two PU surfaces, with and without the coating, taken with a Tencor® Alpha-Step 500 profiler. The two lower images in the same figure show the probability density distribution of the distance between two neighboring peaks from the surface scans. From these plots, it appears as if the coating produced a surface with typical feature size between 10 and 30 μm. The uncoated PU has a broader span in its feature size, and appears to be more random. According to the manufacturer, the coating contains particles of similar size as the feature sizes we measured. It is therefore reasonable to assume that the coating has formed a thin layer of densely packed microscale particles. The stylus (needle) used for the measurements had a radius of 5 μm and a shank[4] angle of 60°. It is therefore reasonable to assume that it was not able to fully resolve all the surface features. The surface heights of the features plotted in Figure 9 are therefore probably somewhat underestimated. Very small features < 5 μm would also be difficult to pick up with our instrumentation.

Initial tests were preformed with the coating to investigate drag reducing properties of the surface. For this test, we employed three identical 25 m long seismic streamer cables with a diameter of 5.5 cm. One cable was coated with the SHS, while the second cable was untreated. The third cable was treated with sand paper to produce an organized surface roughness in the polyurethane with feature sizes around 200 μm. The three cables were submerged for several hours before they were dragged behind a boat at 6 knots approximately 1 m below the surface. The sea was calm during this experiment. The drag force was measured on two identical Sauter FH 1 k force gauges with 0.5 N resolution. Several measurements were taken where we compared two and two cables.

For a seismic streamer in our drag experiment, the Reynolds number based upon streamer diameter $Re_d = U_0 d/\nu$ is $\approx 1.65 * 10^5$. Re_L based on the length of the streamer (L), is in the range of 10^6 to 10^9, while a Reynolds number based on boundary layer thickness Re_δ, is around 10^5 to 10^6. Re_L can also be estimated based on the measured friction drag F_D.

The drag coefficient on our 25 m long seismic streamer cables is

$$C_D = F_D/(\rho U_0^2 \pi 0.5 * dL) \approx 4.45 * 10^{-3}. \qquad (12)$$

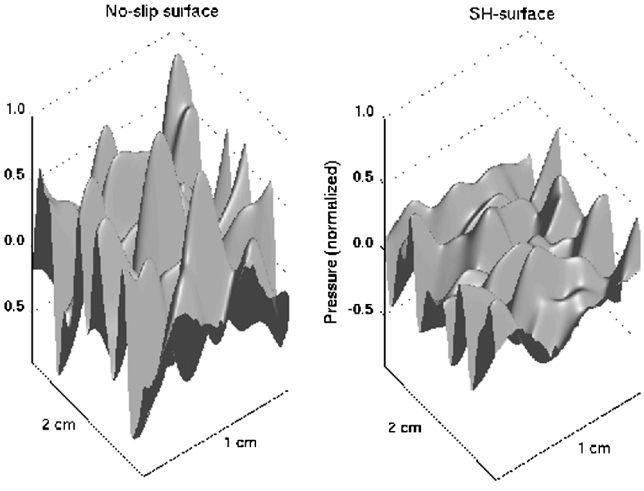

Figure 8. A 2D comparison of the instantaneous far-field pressure (flow noise) outside the no-slip (left) and the SHS slip (right) boundary. The pressure estimates are derived from the numerical simulation of the $Re_\tau = 395$ channel-flow, and the plot has been scaled using the approximation that $x_2^+ = 100$ corresponds to 1 cm.

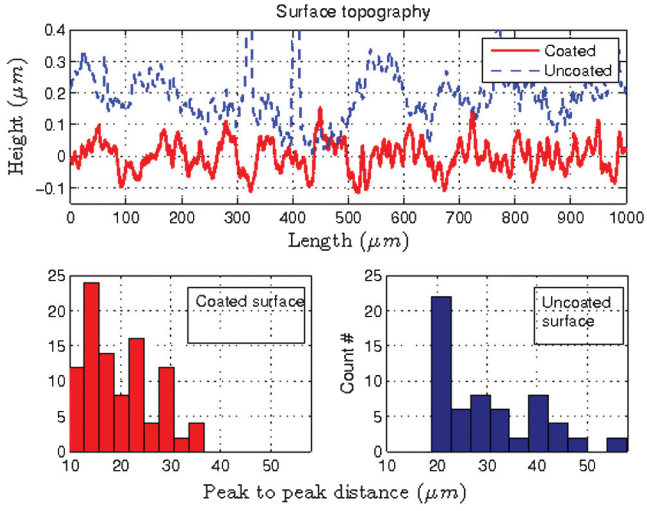

Figure 9. Top image: 1D surface scans of a polyurethane surface with and without the coating. The stapled line (uncoated) has been shifted upwards by 0.2 μm for clarity. Bottom images: Probability density plots of the distances between neighboring peaks from the scans. This is a measure of the surface feature size.

[4]The shank angle describes the shape of the stylus near its tip.

Dette er en postprint-versjon / This is a postprint version.
DOI til publisert versjon / DOI to published version: 10.1190/GEO2011-0001.1

(Note, this also includes 2 m of tow rope). Based on an empirical formula flat plate turbulent flow given by Schlichting (1979), we can estimate $Re_L = 1/(C_D/0.074)^5 \approx 1.2 * 10^6$, which corresponds to an effective length of 0.3–0.4 m. This can be compared with Heenan and Morrison (2002) who argue that typical drag coefficients for streamers indicate an effective length of 2–3 m.

The aim of our second coating experiment was to investigate if the coat also would reduce the amount of flow noise recorded on a streamer. The coat was therefore applied to four hydrophone groups, corresponding to 50 m of streamer, on an ION Digistreamer® cable used for exploration on the Fugro Geoteam AS operated seismic vessel *Geo Arctic*. This streamer cable has an outer diameter of 5.3 cm and consists of hydrophone groups, each with eight individual Teledyne T2BX hydrophones. The output from all hydrophones within each group are summed and recorded on the vessel. Typically, there are 480 groups in a seismic streamer, giving it a total length of 6 km. The vessel was operating in the Barents Sea when the data was acquired. During our experiment, the streamer remained at a depth of around 7 m, and was continuously moving at around 5 knots. On average, four 30s noise recordings were acquired every day during a 30-day period in July and August 2009. The rest of the time the vessel was acquiring normal seismic data. A subset of one of these noise records can be seen in Figure 10. The data was recorded with a 2 ms sampling rate, limiting the maximum frequency to 250 Hz. The hydrophones we use are mounted approximately 1 cm beneath the surface of the streamer, and have a sensor head with a diameter $d \approx 1$ cm. Following Winkel et al. (2008), we estimate the roll-off frequency f_c, where the spectrum is attenuated by 50% due to convolution of the of the signal over the sensor area as $f_c = U_c/2\pi d \approx 55$ Hz. Here, U_c is the convection velocity, which is approximately $2/3$ of the towing velocity.

This indicates that most likely only the low- and midfrequency range of the TBL flow noise was captured. Note that this estimate does not relate to the ability of the hydrophones to pick up far-field reflection data. Such data is recorded up to the Nyquist frequency.

Before any analysis was done, a low-cut filter was applied to attenuate hydrostatic fluctuation noise and swell noise below 2 Hz. The weather was fair (sea state 0–2) during the data acquisition. From the acquired data, we computed spectral estimates and the rms noise levels on a number of traces. These results were then used to compare the coated and the uncoated parts of the streamer.

Sensor calibration

Sensor calibration on seismic hydrophone arrays is performed in two different ways. Absolute calibration is done at the factory where all hydrophone groups are submitted to a known signal, and the response (in Volt per Bar) is measured. In order for a subarray to be accepted, variations in sensitivity between groups are not allowed to exceed ±6%. However, in most cases it is significantly less. The second calibration check is done during operations. It is standard practice within the industry to continuously monitor the rms level of all recorded data. This is done for thousands of shot gathers every day. Averaging these results provides a very accurate and continuous measure of the relative sensitivity of neighboring hydrophone groups. On-board analysis showed that the coating did not change the relative sensitivity to seismic reflection data between the coated and uncoated sections. The coating only seemed to reduce the amount of TBL noise recorded. Figure 10 shows example traces from one of the noise gathers recorded in our experiment.

Variability and repeatability of the measurements

All seismic data are troubled by various types of noise. Generally, we can say that the acoustic environment in the ocean is very rich, and strongly varying. Experience has shown, that during good weather, the average recorded rms noise level seen in seismic data is in the order of 3–4 μBar. However, between individual gathers, both in time and space, it will often vary by 50% or more.

During this experiment, we recorded pure noise for about 2 min every day. Within these records, we then compared the noise level between the coated and the uncoated sections. Due to the strongly varying background noise, the results do not produce smooth lines when they are plotted. Nevertheless, they show clear trends, which is presented in the section below.

RESULTS

The drag experiment

Figure 11 presents the data from our initial drag experiment on three 25 m long seismic streamer cable sections. A total drag reduction of approximately 4% can be observed on the coated cable compared to uncoated cable. It should be noted that during this test, uncoated metal weights were attached along the coated and the uncoated streamer cables to keep them submerged. These weights most likely contributed significantly to the overall drag. The measured 4% drag reduction is therefore probably an underestimation of the drag reducing effect of this particular coating. The third (uncoated) cable with the organized surface roughness was also tested. The result was a 5% *increase* in drag compared to the smooth (untreated) streamer cable.

The noise experiment

Figure 12 is derived from data acquired in the Barents Sea noise experiment. It shows how the SHS coating affected the average rms noise level on four hydrophone groups compared to neighboring uncoated hydrophone groups. To quantify some of the uncertainties, dashed lines were added to Figure 12, which indicate the bounds for one standard deviation. Based upon this, it is reasonable

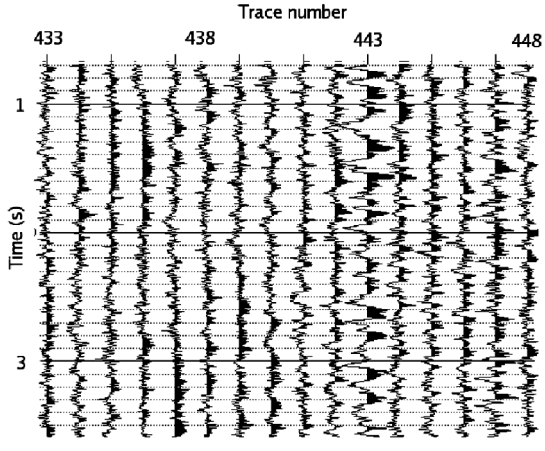

Figure 10. A subset of typical unfiltered noise data recorded during the experiment. Here, traces 433 to 437 are coated with the SHS, while the other traces are uncoated. Trace number 443 stands out because a bird was attached to the streamer close to this channel.

Dette er en postprint-versjon / This is a postprint version.
DOI til publisert versjon / DOI to published version: 10.1190/GEO2011-0001.1

to conclude that initially, the rms noise level was reduced by the SHS-coating by between 7% and 13%. Figure 12 also indicates a relative increase in rms noise level over time. This can most likely be attributed to a degradation of the coating efficiency.

Figure 13 shows power spectrum estimates from the first twenty noise gathers acquired on the seismic streamer used for our Barents Sea seismic recordings (Figure 12). The term "noise gather" is used to describe recording of data on a seismic vessel that does not fire its air guns. If the air-guns are fired the data would be called a "shot," or data gather. These gathers were chosen because they were the ones acquired before the coating failed. The SHS coating mostly seems to have an effect on frequencies below 10 Hz where most of the flow noise is present. In this range, the noise level is reduced by up to 6 dB, which roughly corresponds to halving the amount of noise. Few significant differences are observable above 10 Hz. This reduction in flow noise level is the most important result presented in this work.

Physically, this result can be explained from numerical analysis and drag measurements. The surface coating reduced wall friction and consequently fewer energetic large scale structures were produced in the TBL. As a direct result of this, less low frequency flow noise was produced and recorded.

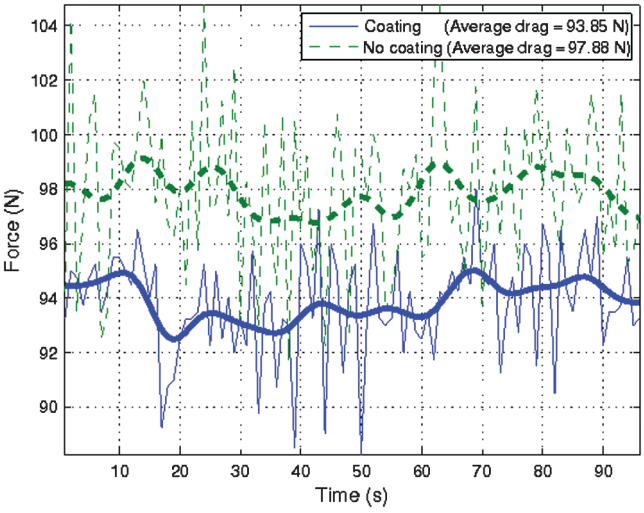

Figure 11. Measured difference in total drag between two 25-m-long streamer cables towed at 6 knots. The thin lines show individual measurements while the thick lines show a moving average. One measurement was taken each second, and the error of the probe is less than 0.5 N.

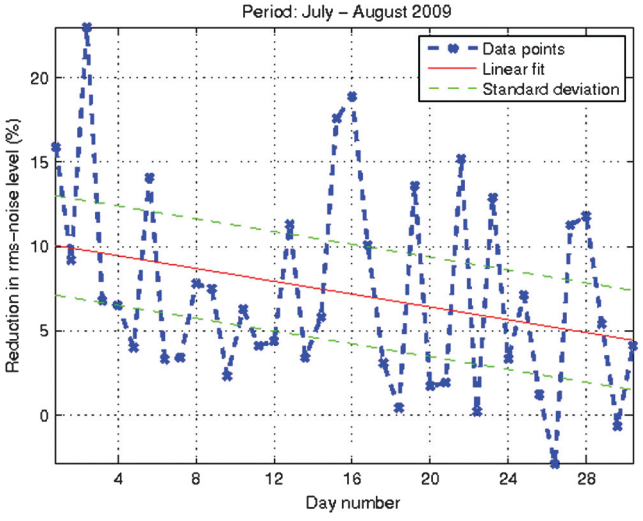

Figure 12. The computed reduction in rms noise level obtained by coating the streamer. The thick dashed line shows the individual data measurements, while the thin solid line represents a linear fit to the data. Two thin dashed lines indicate the bounds to one standard deviation. Initially, the SHS coating reduced the rms noise level by roughly 10%.

DISCUSSION

In marine seismic data, the most common type of noise is what normally referred to as "swell noise." This noise, normally below 10 Hz, increases with sea state. According to Smith (1999), high levels of swell noise can induce delays that account for up to 40% of the total cost of a marine survey. Figure 13 shows that the hydrophobic coating reduced the noise level in this swell noise frequency range. From a commercial point of view, this is interesting.

Figure 12 indicates the effectiveness of the coating is reduced with time. There are several possible explanations for this.

- The coat could be washed off through wear and tear. After around 30 days in the water, the cable was retracted onto the vessel. A few days later it was redeployed into the water, where it stayed for another 30 days. After this redeployment, no noise reducing effect on the coated sections was observed. This indicates that the coating may be destroyed by heavy handling.
- The coating could have been covered by bio-film. In a similar test with a coated streamer section in the ocean off French Guiana in October and November 2009, no noise reducing

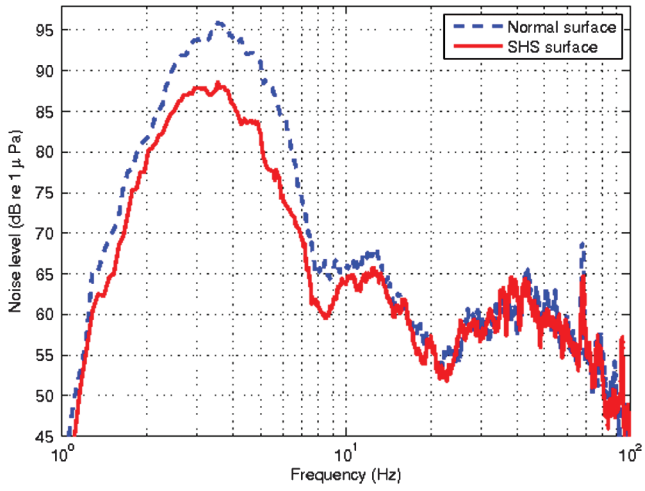

Figure 13. One sided power spectrum estimates from noise gathers recorded on a seismic streamer section. The spectral estimates were obtained by using a multitaper method (Thomson, 1982). The small peak seen close to 70 Hz is probably caused by the towing vessels engine. Note that below 10 Hz, the reduction in flow noise level is up to almost 6 dB. A low-cut filter also has been applied, and has attenuated most of the signal below 2 Hz.

Dette er en postprint-versjon / This is a postprint version.
DOI til publisert versjon / DOI to published version: 10.1190/GEO2011-0001.1

effect of the coating material was detectable when the streamer had been in the water for about three weeks. This was probably because the coating had been covered by a bio-film (fouling). It is fairly common that seismic streamer cables that are subjected to long term deployment in tropical waters become covered by a bio-film. No fouling was visible on the cable used in the Barents Sea (arctic water). Nevertheless, a thin layer of biological materials could have avoided detection by the crew.

- Under high Reynolds number flows SHS, coatings could theoretically lose the air pockets within the structure due to increased pressure fluctuations occurring on decreasing length scales, as well as the dissolving of the air into the water. Consequently, it is possible that the rewetting of the surface could be partially responsible for the decreased performance over time.

If rewetting occurs, the drag and noise reduction observed in our experiments could be caused by other not yet understood phenomena. The coating did cover the polyurethane surface, and could potentially have made this surface more smooth. However, even untreated streamer skin appear to be smooth (see Figure 9), so it is doubtful that this alone could explain the results. In Woolford et al. (2009), no discernible slip velocity was measured over a SHS surface in turbulent flow. However, they still measured a significant reduction in the friction coefficient in their pipe flow. A theoretical analysis by Fukagata et al. (2006) proposes an explanation of how a small alteration of the laminar sublayer by a SHS can affect the entire TBL and subsequently alter the drag. This could explain our results. We also speculate that some of the very small scale surface features (<10 μm) seen in Figure 9 are able to retain pockets of air, even at the high Reynolds numbers experienced on a seismic streamer.

In the future, we plan a number of experiments where we combine a highly hydrophobic surface coating with anti fouling additives. Hopefully, this will enable us to say more about whether the reduction in effect of coating with time is due to washing off, fouling, or rewetting.

CONCLUSIONS

This paper presented measurements which demonstrated that a hydrophobic surface coat reduced the overall rms flow noise level on a commercial seismic streamer cable section by approximately 10%. The same coating also reduced the cable drag in an ocean environment by roughly 5%.

Although a 10% reduction in noise level appears small, seismic streamer technology has been fine-tuned over many decades to improve the S/N and any improvement is significant. It should be noted that for frequencies below 10 Hz, SHS reduced the noise level by nearly 6 dB corresponding to 50%. This is very significant, since in seismic surveys, it is the noise encountered at these low frequencies that cause most problems, and often results in the need to reacquire the data.

To gain a better physical understanding of drag and flow noise reduction, a database of DNS of flow over SHS was employed. These simulations used an idealized SHS and resulted in an rms flow noise reduction of nearly 60%. As in the measured data, most of this reduction was at relative low frequencies, where also most of the flow noise can be found. Such a large reduction is difficult to achieve in an industrial application. However, this result provided a theoretical upper limit and a guide for future research and development.

Our analysis of the computer simulations also provided an improved understanding of where most acoustic noise is produced in a turbulent flow. In most cases, flow noise is only produced in a thin layer $x_2^+ < 50$ above a surface. In real-life flows over seismic streamers, this corresponds to just a few *mm*.

Furthermore, our analysis of the numerical simulation data showed that the kinematic structure of the turbulence is changed by the SHS. Near this surface the turbulence seems to approach a 1C limit in which the magnitude of one fluctuation is significantly larger than the other two. Physically this implies that there is less turbulent mixing of momentum in the wall-normal direction close to the slip boundary. Consequently less high-speed flow from the outer regions is brought into the low-speed near-wall region and the viscous drag is reduced.

Finally, we mention that the coating material tested appears to have a limited lifetime and fails after one or more months in the water. In spite of these shortcomings, our measurements have shown that SHS possesses significant drag and flow noise reduction potential. Future work will include efforts to significantly extend the durability of SHS coatings on seismic streamer cables.

ACKNOWLEDGMENTS

The authors want to thank H. Steen, B. B Johnsen, and T. R. Frømyr at FFI, H. J. Aakre at Fugro, and R. Meyer at Nanoconcept for help with the measurement work. The crew on the seismic vessel *Geo Arctic* are also acknowledged for their aide. Finally, thanks to the reviewers for their valuable comments that helped improve the quality of this paper. This work was supported by the Norwegian Research Council through Grant PETROMAKS 175921/S30 and by Fugro.

REFERENCES

Barker, S. J., 1973, Radiated noise from turbulent boundary layers in dilute polymer solutions: Physics of Fluids, **16**, no. 9, 1387–1394, doi: 10.1063/1.1694530.

Barthlott, W., and N. Ehler, 1977, Electronmicroscopic images of the surfaces of spermatophyten (English translation): Tropische und subtropische Pflanzenwelt (Akad. Wiss. Lit. Mainz), **19**, 110.

Bechert, D. W., M. Bruse, W. Hage, J. G. T. van der Hoeven, and G. Hoppe, 1997, Experiments on drag-reducing surfaces and their optimization with an adjustable geometry: Journal of Fluid Mechanics, **338**, no. 1, 59–87, doi: 10.1017/S0022112096004673.

Berenger, J.-P., 1994, A perfectly matched layer for the absorption of electromagnetic waves: Journal of Computational Physics, **114**, 185–200, doi: 10.1006/jcph.1994.1159.

Bjelland, C., 1993, Reduction of noise in seismic hydrophone arrays modeling of breathing waves and adaptive noise canceling: Ph.D. thesis, University of Bergen, Norway.

Brungart, T. A., W. J. Holmberg, A. A. Fontaine, S. Deutsch, and H. L. Petrie, 2000, The scaling of the wall pressure fluctuations in polymer-modified turbulent boundary layer flow: The Journal of the Acoustical Society of America, **108**, no. 1, 71–75, doi: 10.1121/1.429445.

Choi, K., 1987, A new look at the near-wall turbulence structure: Advances in turbulence: Springer Verlag, 373–382.

Cipolla, K. M., and W. L. Keith, 2008, Measurements of the wall pressure spectra on a full-scale experimental towed array: Ocean Engineering, **35**, no. 10, 1052–1059, doi: 10.1016/j.oceaneng.2008.02.006.

Daniello, R. J., N. E. Waterhouse, and J. P. Rothstein, 2009, Drag reduction in turbulent flows over superhydrophobic surfaces: Physics of Fluids, **21**, no. 8, 085103, doi: 10.1063/1.3207885.

Dowling, A., 1998, Underwater flow noise: Theoretical and Computational Fluid Dynamics, **10**, no. 2, 135–153, doi: 10.1007/s001620050055.

Elbing, B. R., E. S. Winkel, S. L. Ceccio, M. Perlin, and D. R. Dowling, 2010, High-reynolds-number turbulent-boundary-layer wall-pressure

fluctuations with dilute polymer solutions: Physics of Fluids, **22**, no. 8, 085104, doi: 10.1063/1.3478982.
Elbing, B. R., E. S. Winkel, K. A. Lay, S. L. Ceccio, D. R. Dowlling, and M. Perlin, 2008, Bubble-induced skin-friction drag reduction and the abrupt transition to air-layer drag reduction: Journal of Fluid Mechanics, **612**, 201–236, doi: 10.1017/S0022112008003029.
Elboth, T., D. Lilja, B. A. Pettersson-Reif, and Ø. Andreassen, 2010, Investigation of flow and flow noise around a seismic streamer cable: Geophysics, **75**, no. 1, Q1–Q9, doi: 10.1190/1.3294639.
Frohnapfel, B., P. Lammers, J. Jovanović, and F. Durst, 2007, Interpretation of the mechanism associated with turbulent drag reduction in terms of anisotropy invariants: Journal of Fluid Mechanics, **577**, 457–466, doi: 10.1017/S0022112007005083.
Fukagata, K., N. Kasagi, and P. Koumoutsakos, 2006, A theoretical prediction of friction drag reduction in turbulent flow by superhydrophobic surfaces: Physics of Fluids, **18**, no. 5, 051703, doi: 10.1063/1.2205307.
Fulton, T., 1985, Some interesting seismic noise: The Leading Edge, **4**, 70–75, doi: 10.1190/1.1439183.
Gogte, S., P. Vorobieff, R. Truesdell, A. M. li, F. van Swol, P. Shah, and C. J. Brinker, 2005, Effective slip on textured superhydrophobic surfaces: Physics of Fluids, **17**, no. 5, 051701, doi: 10.1063/1.1896405.
Haddle, G. P., 1969, The physics of flow noise: Journal of the Acoustical Society of America, **46**, no. 1B, 130–157, doi: 10.1121/1.1911663.
Hahn, S., J. Je, and H. Choi, 2002, Direct numerical simulation of turbulent channel flow with permeable walls: Journal of Fluid Mechanics, **450**, 259–285, doi: 10.1017/S0022112001006437.
Heenan, A. F., and J. F. Morrison, 2002, Turbulent boundary layers on axially-inclined cylinders. II. Circumferentially averaged wall-pressure wavenumber-frequency spectra: Experiments in Fluids, **32**, no. 6, 616–623, doi: 10.1007/s00348-001-0385-4.
Henoch, C., T. N. Krupenkin, P. Kolodner, J. A. Taylor, M. S. Hodes, and A. M. Lyons, 2006, Turbulent drag reduction using superhydrophobic surfaces: 3rd AIAA Flow Control Conference, 3192–3196.
Kerman, B. R., 1984, Underwater sound generation by breaking wind waves: Journal of the Acoustical Society of America, **75**, no. 1, 149–165, doi: 10.1121/1.390409.
Kjellgren, P., and L. Davidson, 2009, Large eddy simulations of turbulent flow noise on streamers: 79th Annual International Meeting, SEG, Expanded Abstracts, 117–121.
Knight, A., 1996, Flow noise calculations for extended hydrophones in fluid- and solid-filled towed arrays: Journal of the Acoustical Society of America, **100**, no. 1, 245–251, doi: 10.1121/1.415891.
Landau, L. D., and E. M. Lifshitz, 1987, Fluid mechanics, 2nd ed., Course of theoretical physics vol. **6**, §75.
Lighthill, J., 1952, On sound generated aerodynamically. I. General theory: Proceedings of the Royal Society of London B, **211**, no. 1107, 564–587.
Lighthill, J., 1954, On sound generated aerodynamically. II. Turbulence as a source of sound: Proceedings of the Royal Society of London B, **222**, no. 1148, 1–32.
Lumley, J. L., 1978, Computational modelling of turbulent flow: Advances in Applied Mechanics, **18**, A79-47538 21-34, 123–176, doi: 10.1016/S0065-2156(08)70266-7.
Lumley, J. L., and G. Newman, 1977, The return to isotropy of homogeneous turbulence: Journal of Fluid Mechanics, **82**, no. 1, 161–178, doi: 10.1017/S0022112077000585.
Ma, M., and R. M. Hill, 2006, Superhydrophobic surfaces: Current Opinion in Colloid & Interface Science, **11**, 193–202, doi: 10.1016/j.cocis.2006.06.002.
Martell, M. B., 2009, Simulation of turbulence over superhydrophobic surfaces: Master's thesis, University of Massachusetts Amherst.
Martell, M. B., J. B. Perot, and J. P. Rothstein, 2009, Direct numerical simulations of turbulent flows over drag reducing ultrahydrophobic surfaces: Journal of Fluid Mechanics, **620**, 31–41, doi: 10.1017/S0022112008004916.
Martell, M. B., J. P. Rothstein, and J. B. Perot, 2010, An analysis of superhydrophobic turbulent drag reduction mechanisms using direct numerical simulation: Physics of Fluids, **22**, 065102, 065102, doi: 10.1063/1.3432514.
McDonald, M. A., J. A. Hildebrand, S. M. Wiggins, and D. Ross, 2008, A 50 year comparison of ambient ocean noise near San Clemente Island: A bathymetrically complex coastal region off southern California: Journal of the Acoustical Society of America, **124**, no. 4, 1985–1992.
Nishi, R. Y., 1970, Measurement of noise on an underwater towed body: Journal of the Acoustical Society of America, **48**, no. 3B, 753–758.
Peacock, J. H., C. G. Sykes, N. W. Cameron, and L. G. Peardon, 1983, Advanced acoustic design for a new seismic streamer: 53rd Annual international Meeting, SEG, Expanded Abstracts, **465**, 465–466.
Sanders, W. C., E. S. Winkel, D. R. Dowlling, M. Perlin, and S. L. Ceccio, 2006, Bubble friction drag reduction in a high-reynolds-number flat-plate turbulent boundary layer: Journal of Fluid Mechanics, **552**, 353–380, doi: 10.1017/S0022112006008688.
Schlichting, H., 1979, Boundary layer theory: McGrawHill.
Schoenberger, M., and J. F. Mifsud, 1974, Hydrophone streamer noise: Geophysics, **39**, 781–793, doi: 10.1190/1.1440466.
Smith, J. G., 1999, Amplitude and phase effects of weather noise: 69th Annual International Meeting, SEG, Expanded Abstracts, 1485–1488.
Solbakken, S., and H. I. Andersson, 2004, On the drag reduction mechanism in a lubricated turbulent channel flow: International Journal of Heat and Fluid Flow, **25**, no. 4, 618–624, doi: 10.1016/j.ijheatfluidflow.2004.03.001.
Thomson, D., 1982, Spectrum estimation and harmonic analysis: Proceedings of the IEEE, **70**, 1055–1096, doi: 10.1109/PROC.1982.12433.
Wenz, G. M., 1962, Acoustic ambient noise in the ocean: Spectra and sources: Journal of the Acoustical Society of America, **34**, no. 12, 1936–1950.
Winkel, E. S., B. R. Elbing, S. L. Ceccio, M. Perlin, and D. R. Dowling, 2008, High-reynolds-number turbulent-boundary-layer wall pressure fluctuations with skin-friction reduction by air injection: The Journal of the Acoustical Society of America, **123**, no. 5, 2522–2530, doi: 10.1121/1.2902169.
Woolford, B., J. Prince, D. Maynes, and B. W. Webb, 2009, Particle image velocimetry characterization of turbulent channel flow with rib patterned superhydrophobic walls: Physics of Fluids, **21**, no. 8, 085106–085106–12, doi: 10.1063/1.3213607.

Dette er en postprint-versjon / This is a postprint version.
DOI til publisert versjon / DOI to published version: 10.1190/GEO2011-0001.1